

Restriction Model Independent Method for Non-Isentropic Outflow Valve Boundary Problem Resolution

Felipe Castillo
Renault, France

Emmanuel Witrant, Luc Dugard
Gipsa Lab, Grenoble France

Vincent Talon
Renault, France

Copyright © 2012 Society of Automotive Engineers, Inc.

ABSTRACT

To meet the new engine regulations, increasingly sophisticated engine alternative combustion modes have been developed in order to achieve simultaneously the emission regulations and the required engine drivability. However, these new approaches require more complex, reliable and precise control systems and technologies. The 0-D model based control systems have proved to be successful in many applications, but as the complexity of the engines increases, their limitations start to affect the engine control performance. One of these limitations is their inability to model mass transport time. 1-D modeling allows some of the 0-D models limitations to be overcome, which is the motivation of this work.

In this paper, two quasi-steady outflow boundary models are developed: One based on the isentropic contraction and another based on a momentum conservation approach. Both are compared with the results of computational fluid dynamics (CFD) 3-D simulations. Then, an innovative method for solving the outflow boundary problem taking into account the entropy correction at the boundary for a 1-D unsteady gas flow modeling is presented. This method permits the boundary problem to be solved independently of the restriction model, which is typically captured in the resolution method. It means that a physical restriction model can be modified without needing to change the boundary resolution method. A Newton-Raphson algorithm is used with a modified Method of Characteristics (MOC) scheme to solve the boundary problem along with an extrapolation for the initialization of the scheme, which reduces the calculation time and increases the solution accuracy. Additionally, the

performance of the proposed method is compared with the scheme presented in the literature and the method for solving the unsteady state is validated using a GT-Power model as reference.

INTRODUCTION

In the recent years, Diesel engine emissions regulations have become stricter while preserving the performance of the engine. Although significant improvements have been made over the past years, there are still many challenges that need to be overcome in order to meet the future emission regulations. The introduction of sophisticated alternative combustion modes such as homogeneous charge compression ignition (HCCI), low temperature combustion (LTC) and premixed controlled compression ignition (PCCI) offer a great potential to reduce the engine emission levels [1] [2] [3]. However, these new modes require different fueling strategies and in-cylinder conditions, thus creating the need for more complex, reliable and precise control systems and technologies.

Dual-loop exhaust gas recirculation (EGR) with both high and low-pressure recirculations is one of the new strategies proposed to achieve the appropriate conditions to implement multiple combustion modes [4]. However, ensuring the adequate in-cylinder conditions is still a very difficult task, as the introduction of the EGR brings many control challenges due to the lack of EGR flow rates and mass fraction measurements. An efficient control of the in-cylinder combustion and engine-out emissions not only involves the total in-cylinder EGR amount, but also the ratio between the

high pressure EGR (HP-EGR) and the low pressure EGR (LP-EGR). Indeed, this ratio is crucial as the gas temperatures and compositions are significantly affected. The HP-EGR gas is helpful to stabilize the combustion at low load since its temperature is high. The LP-EGR reduces the engine-out NOx emission without excessive smoke as it is filtered by the particle filter. Controlling the air fractions in the intake manifold is an efficient approach to control the in-cylinder EGR amount [5] [6]. For engines with dual EGR systems, the air fraction upstream of the compressor indicates the LP-EGR rate and the air fraction in the intake manifold indicates the total EGR rate. Therefore, if the air fractions in each section are controlled well, then the HP and LP-EGR can be well controlled.

Nevertheless, controlling the air mass fraction is a difficult task, as direct measurement of the air fraction is not available on the production engines and as the dynamics of the admission air-path can be highly complex. One of the actual problems to control the air mass fraction in the intake manifold is the EGR mass transport time. This phenomenon is much more significant in the LP-EGR as the distance that the gas has to travel is much longer than the one associated with HP-EGR. Indeed, this phenomenon causes a degradation of the overall engine emission performance during the strong transients. Several air mass fraction/EGR rate estimation methods have been proposed in the literature to overcome some of the actual limitations [7] [8] [6]. However, most of these estimation techniques are based on 0-D engine modeling, which does not permit to take into account the mass transport time.

In this paper, a 1-D aerodynamics modeling platform is developed in order to provide an accurate white box model to synthesize and validate control laws and estimators that are able to take into account the mass transport time. The study detailed in this paper is focused on the cylinder intake valve model. The mathematical modeling of 1-D unsteady gas flow in a pipe system is based on Euler's equations. In order to solve the cylinder inlet valve boundary condition, a specific resolution of Euler's equations need to be implemented. In this case, due to its satisfying robustness and accuracy, a method of characteristics modified to take into account the non-homentropic flows through the intake valves is implemented.

Our paper is organized as follows. First, the equations and hypotheses introduced to build intake valve models are described. A classical quasi-steady one-dimensional outflow model is developed along with an alternative momentum-based quasi-steady outflow model. Both models are compared with CFD 3-D

simulation results.

Then, a modified MOC is proposed to develop an innovative non-homentropic outflow boundary resolution methodology that allows to implement different outflow models without modifying the boundary resolution scheme. Additionally, a Newton-Raphson algorithm is introduced in the scheme, along with an extrapolation to initialize the resolution method. It reduces the calculation time and increases the accuracy.

Finally, the performance of the proposed scheme is compared with traditional approaches and an unsteady validation of the scheme is done using GT-Power as reference.

MOTIVATION

A simple example illustrates the problematic that actually exists in the control of the air mass fraction in the intake manifold when a sudden change of the LP-EGR rate occurs. The system shown in Figure 1 consists in a tube with restriction on both ends. At the left end, there is known a pressure p_{in} , a known temperature T_{in} and a known air mass fraction F_{in} . Assume that the system is in steady state at time 0. Then, a sudden change of F_{in} (from 0 to 1) is introduced at time 0 at the left end and the response is simulated using a 0-D and a 1-D model. The results obtained are presented in Figure 2.

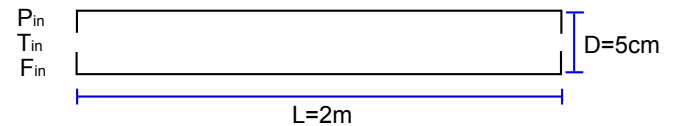


Figure 1: System used to carry out the 0-D and 1-D approaches comparison

As depicted in Figure 2, there is an important difference between the response obtained with the 0-D model and the one with the 1-D model. For example, the 0-D model over-estimates the air mass fraction between 0 and 0.1 seconds (transient phase), which would compromise the engine NOx emission performance in that time interval. The 1-D model response presents a more realistic behavior of the air mass fraction during the transient response, as it takes into account the mass transport time. This example illustrates the potential of using 1-D models to synthesize control laws and observers that are efficient during the transients.

QUASI-STEADY RESTRICTED OUTFLOW MODELS

In this section, the equations and assumptions from literature outflow models are derived along with a

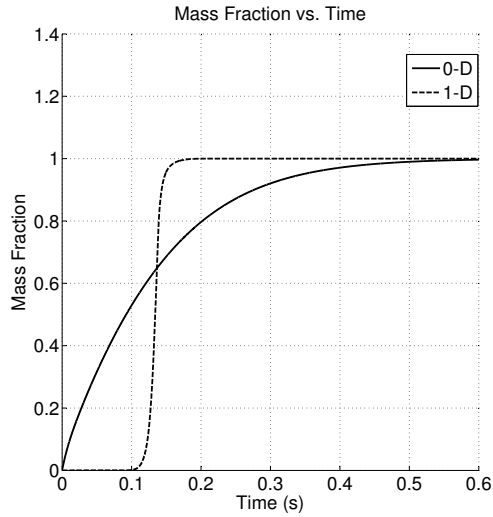


Figure 2: Right tube end air mass fraction of the 0-D and 1-D models in response to a unit step input air mass fraction.

model based on the momentum equation instead of the isentropic contraction. Figure 3 depicts an outflow restricted boundary where three quasi-stationary planes have been defined. The plane 0 represents the stagnation state, the plane 1 is located just before the restriction and the plane 2 is located in the restriction throat. The gas exits the pipe by the restriction throat as a jet of cross-sectional area C_2 . There are six unknown quantities: the pressure p , the velocity u and the density ρ at planes 1 and 2. Hence, six equations are needed in order to solve the boundary problem. At the time when these models were developed, desktop computers memory did not allow to pre-calculate solutions into data-maps. Indeed, Newton-Raphson algorithms were used to solve the boundary problem, introducing an iterative problem at each time step. The main issue of this approach is that the convergence algorithm had to be modified for each specific model. Pre-processed data-maps at the interface between the quasi-steady model and the 1-D Lax-Wendroff are thus advantageous. Therefore, all the models developed in this section are put into data-maps.

Most approaches that are used to solve the outflow restriction boundary problem assume to have an isentropic contraction between plane 1 and 2 (e.g see Benson's proposal) [9] [10]. However, there has been other propositions such as [11], where a polytropic constant found through a data-map is proposed in order to create a non-homentropic approach, allowing to use the same formulation as the homentropic case. Consequently, the same overall boundary problem resolution process can be used. In this section, an additional method to create data-maps inspired from a momentum approach is presented and then compared

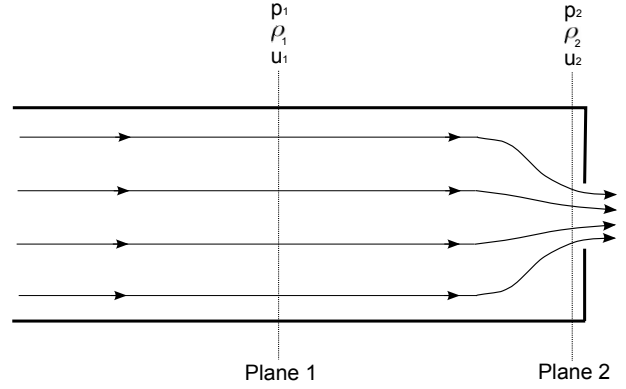


Figure 3: Outflow Restriction Schema

with the traditional isentropic contraction approach and 3-D CFD steady state results. The purpose of this section is to illustrate some physical outflow restriction models that can be obtained and the interest of generating a unique boundary resolution method.

OUTFLOW MODEL USING THE ISENTROPIC CONTRACTION EQUATION

The following assumptions are made in order to create the model:

- A-1 under subsonic conditions, the back-pressure p_b at plane 0 is equal to the pressure at the throat meaning $p_b = p_2$ (no allowance is made for the pressure recovery);
- A-2 the state is quasi-steady over the three planes;
- A-3 the contraction is isentropic between planes 1 and 2.

To start the development of this classical data-map building method, three basic equations are used: energy conservation, mass conservation and isentropic contraction (A-3). These equations write respectively as follows [10]:

$$a_{tot}^2 = a_1^2 + \frac{\gamma-1}{2} u_1^2 = a_2^2 + \frac{\gamma-1}{2} u_2^2 \quad (1)$$

$$\frac{p_1}{p_2} = \Phi \frac{u_2}{u_1} \left(\frac{a_1}{a_2} \right)^2 \quad (2)$$

$$\frac{p_1}{p_2} = \left(\frac{a_1}{a_2} \right)^{\frac{2\gamma}{\gamma-1}} \quad (3)$$

where a is the sound speed, u is the particle speed, $a_{tot} = \sqrt{a^2 + \frac{\gamma-1}{2}u^2}$ is the total sound speed, γ is the specific heat ratio and $\Phi = \frac{C_2}{C_1}$ the sectional ratio. Combining (2) and (3) gives:

$$\left(\left(\frac{a_1}{a_2}\right)^2\right)^{\frac{\gamma}{\gamma-1}} = \Phi \frac{u_2}{u_1} \left(\frac{a_1}{a_2}\right)^2 \quad (4)$$

The energy equation (1) can be written as:

$$\left(\frac{a_1}{a_2}\right)^2 = \left(\frac{a_{tot}}{a_2}\right)^2 - \frac{\gamma-1}{2} \left(\frac{u_1}{a_2}\right)^2 \quad (5)$$

Replacing (5) in (4) and defining the non-dimensional speeds as $A = \frac{a}{a_{tot}}$ and $U = \frac{u}{a_{tot}}$.

$$U_1 = \Phi U_2 \left[\left(\frac{1}{A_2}\right)^2 - \frac{\gamma-1}{2} \left(\frac{U_1}{A_2}\right)^2 \right]^{\frac{-1}{\gamma-1}} \quad (6)$$

This equation provides a static relationship between the speed at the throat U_2 and the speed at the boundary U_1 . A_2 can be written in terms of U_2 and A_1 in terms of U_1 using the energy conservation equation (1). With (3), a relationship between U_1 and the pressure ratio $\frac{p_1}{p_2}$ is found, which is what is finally captured in the data-map. However, this is only valid for sub-sonic flows and a complementary analysis has to be performed for the sonic flow case.

Under sonic conditions the particle speed equals to the sound speed, which implies from (1) that $U_2 = A_2 = \sqrt{\frac{2}{\gamma+1}}$. Using this result in (6), the critical non-dimensional particle speed U_{1cr} is found as:

$$U_{1cr} = \Phi \sqrt{\frac{2}{\gamma+1}} \left[\left(\frac{\gamma+1}{2}\right) - \frac{\gamma^2-1}{4} (U_{1cr})^2 \right]^{\frac{-1}{\gamma-1}} \quad (7)$$

It is important to notice that U_1 under sonic conditions is independent on the pressure ratio $\frac{p_1}{p_b}$. It only depends on the area ratio $\Phi = \frac{C_2}{C_1}$. The critical pressure ratio p_{cr} , at which the flow becomes sonic can be expressed as:

$$p_{cr} = \left(\frac{\gamma+1}{2}\right)^{\frac{\gamma}{\gamma-1}} (A_{1cr})^{\frac{2\gamma}{\gamma-1}} \quad (8)$$

where A_{1cr} is found using the energy conservation and (7). (8) allows to determine whether the flow is sonic. At this point, all the required information to build the data-map is available. In order to obtain the data-map, the following procedure is proposed:

1. setting a range of U_2 equals to $\left[0, \sqrt{\frac{2}{\gamma+1}}\right]$ (Subsonic range), A_2 is found using (1);
2. now that U_2 and A_2 are generated, (6) solved numerically can be employed to find U_1 . To find A_1 use the energy equation once again;
3. Using 3, the values of $\frac{p_1}{p_0}$ can be found for the subsonic range with the assumption A-1;
4. to include the sonic range in the data map, use the critical pressure ratio p_{cr} . If $\frac{p_1}{p_0} > p_{cr}(\Phi)$, set $U_1 = U_{1cr}(\Phi)$ using 7.

OUTFLOW MODEL USING A MOMENTUM BASED EQUATION

In this subsection, a momentum-based outflow data-map is developed. Figure 4 presents a control volume description to formulate the momentum equation at the boundary.

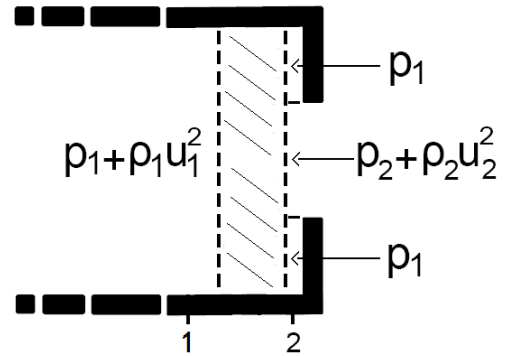


Figure 4: Proposed pressure distribution for the momentum approach

A control volume is once again created between Planes 1 and 2. However, this time there is a particular quantity distribution on Plane 2 that allows to formulate the momentum equation. There are three sections defined in Plane 2: two sections right in front of the restriction walls and one facing the restriction throat (see Figure 4). Some assumptions are made on Plane 2 in order to define all the quantities at each section.

- H-1 u_2 normal to the restriction wall at Plane 2 is zero.
- H-2 The pressure and speed on Plane 2 right next to the throat are p_2 and u_2 respectively.

H-3 The pressure right next to the restriction on plane 2 is equal to p_1 .

All the information required to build the model is now available. The momentum conservation in the virtual control volume shown in Figure 4 implies that:

$$p_1 C_1 - p_2 C_2 - p_1 (C_1 - C_2) = \rho_2 u_2^2 C_2 - \rho_1 u_1^2 C_1 \quad (9)$$

To start with the data-map generation procedure, the sound speed equation $a = \sqrt{\frac{\gamma p}{\rho}}$ and (9) are combined to obtain:

$$\frac{p_2}{p_1} = \left(\frac{1 + \gamma \left(\frac{u_2}{a_2} \right)^2}{1 + \frac{\gamma}{\Phi} \left(\frac{u_1}{a_1} \right)^2} \right) \quad (10)$$

The goal is to express U_1 as a function of U_2 and A_2 , similarly to the previous approach. Combining the mass conservation with (10) gives:

$$\Phi \frac{u_2}{u_1} \frac{a_1^2}{a_2^2} = \left(\frac{1 + \gamma \left(\frac{u_2}{a_2} \right)^2}{1 + \frac{\gamma}{\Phi} \left(\frac{u_1}{a_1} \right)^2} \right) \quad (11)$$

$$\Leftrightarrow \Phi \frac{u_2}{u_1} \frac{a_1^2}{a_2^2} + \gamma \frac{u_2}{a_2^2} u_1 = 1 + \gamma \left(\frac{u_2}{a_2} \right)^2$$

Using the energy conservation (5) and factorizing to obtain a quadratic function of U_1 gives:

$$\left(\gamma - \Phi \frac{\gamma - 1}{2} \right) U_1^2 - \left(\frac{A_2^2}{U_2} + \gamma U_2 \right) U_1 + \Phi = 0 \quad (12)$$

Equations (10) and (12) permit to create the data-map using this momentum-based approach. As done in the literature approach, it is necessary to analyze the sonic flow case. This case is characterized by $A_2 = U_2 = \sqrt{\frac{2}{\gamma + 1}}$, which provides U_1 under sonic conditions as:

$$\left(\gamma - \Phi \frac{\gamma - 1}{2} \right) U_{1cr}^2 - \sqrt{2(\gamma + 1)} U_{1cr} + \Phi = 0 \quad (13)$$

And the pressure ratio under sonic flow is expressed as:

$$p_{1cr} = \left(\frac{1 + \gamma}{1 + \frac{\gamma}{\Phi} \left(\frac{U_{1cr}}{A_{1cr}} \right)^2} \right) \quad (14)$$

Similarly to the isentropic data-map procedure, U_1 under sonic conditions does not depend on the pressure ratio $\frac{p_2}{p_1}$ but only on Φ . The procedure to generate the data-map is presented as follows:

1. setting a range of U_2 equals to $\left[0, \sqrt{\frac{2}{\gamma + 1}} \right]$ (subsonic range), then find A_2 using (1);
2. from U_2 and A_2 , (12) can be employed to find U_1 and A_1 is given by the energy equation;
3. using (10), the subsonic values of $\frac{p_1}{p_0}$ are found (from the assumption A-1);
4. to include the sonic range in the data-map, use the critique pressure ratio p_{cr} : If $\frac{p_1}{p_0} > p_{cr}(\Phi)$ then set $U_1 = U_{1cr}(\Phi)$ from (13).

OUTFLOW MODELS COMPARISON

Figure 5 shows the isentropic and the momentum approach data-maps plotted together in order to evaluate their differences. Additionally, the results obtained using steady-state CFD 3-D simulation (Fluent) are shown with the purpose of illustrating the predictability of each model. Figure 5 shows how the non-dimensional flow velocities are systematically higher in the model using isentropic contraction than in the momentum-based development. This behavior occurs because the isentropic contraction approach does not take into account the increase of entropy through the restriction, which allows for greater flow speeds.

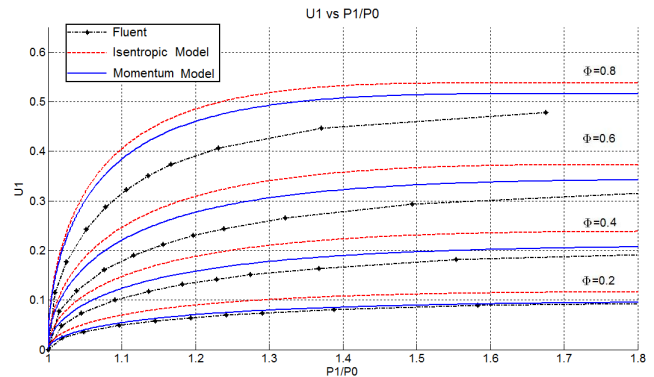


Figure 5: Steady flow results comparison between outflow boundary restriction models

in comparison with the change along the whole tube. On the other hand, the variation of entropy level can be significant, that's why the Riemann invariant for the outflow case is modified as follows [10]:

$$\lambda_{LC} = \lambda_L + A_D^{n+1} \frac{A_{AD}^{n+1} - A_{AL}^n}{A_{AD}^{n+1}} = A_D^{n+1} - \left(\frac{\gamma - 1}{2} \right) U_D^{n+1} \quad (17)$$

where A_A is the entropy level defined as:

$$\left(\frac{p}{p_{ref}} \right)^{\frac{\gamma-1}{2\gamma}} = \frac{A}{A_A} \quad (18)$$

Entropy correction

As previously shown, a modification of the MOC is done in order to take into account the entropy variation at the boundary. A treatment of (17) is performed with the purpose of suppressing the need for defining the traditionally used pressure and sound speed references and allowing the entropy correction to be written directly in terms of the available quantities at time n . Equation (17) can be written as:

$$u_D^{n+1} = \frac{2}{\gamma - 1} (\lambda_{LC} - a_D^{n+1}) \quad (19)$$

Which is expressed in terms of entropy levels as:

$$u_D^{n+1} = \frac{2}{\gamma - 1} \left(\lambda_L^n + a_D^{n+1} \left(1 - \frac{A_{AL}^n}{A_{AD}^{n+1}} \right) - a_D^{n+1} \right) \quad (20)$$

Replacing in (19) the entropy levels by 18 gives:

$$u_D^{n+1} = \frac{2}{\gamma - 1} \left(\lambda_L^n - a_L^n \left(\frac{p_D^{n+1}}{p_L^n} \right)^{\frac{\gamma-1}{2\gamma}} \right) \quad (21)$$

This equation gives a direct relationship between p_D and u_D as λ_L , a_L and p_L are known at time n .

Resolution method

In this part, the proposed resolution method is explained in details. As depicted in Figure 6, there is a second trajectory that takes into account the path along the particle speed u . Along this trajectory, the entropy level

does not change as the heat losses and friction have been neglected for one finite element. Equation (16) represents the information obtained at the boundary from the trajectory u . Knowing that under isentropic conditions

$$\frac{p}{\rho^\gamma} = constant \quad (22)$$

and replacing ρ by the sound speed equation $\rho = \frac{\gamma p}{a^2}$ the following is obtained:

$$\frac{p^{(1-\gamma)} a^{2\gamma}}{\gamma^\gamma} = constant \quad (23)$$

The value of (22) at the point S is denoted as S_s and calculated by a linear interpolation [10]. Equation (16) can be reformulated using the value of S_s and quantities previously defined:

$$a_D = \sqrt{\gamma S_s^{\frac{1}{\gamma}} p_D^{\frac{\gamma-1}{2\gamma}}} \quad (24)$$

This equation relates directly the pressure with the sound speed at the boundary using the information coming from the trajectory u . Equation (21) also relates directly the pressure and the particle speed at the boundary. Therefore, knowing the pressure means solving the whole boundary problem due to the information coming from the Riemann invariants. However, in order to determine the value of the pressure at the boundary, the outflow boundary models developed in the previous section have to be taken into account.

As the interest of this study is to establish a resolution method independently of the chosen outflow model, the relation between the non-dimensional particle speed and the pressure ratio is described by a data-map, such as the ones developed in the previous section, instead of an analytical equation. Hence, the outflow models can be expressed as:

$$PR = datamap(U_D, \Phi) \quad (25)$$

where PR is the pressure ratio $\frac{p_D}{p_b}$, p_b being the known back pressure at the stagnation state. Note that there is an algebraic loop in this formulation because the pressure is required to calculate the particle speed and the particle speed has to be known in order to calculate

the pressure. A numerical procedure is thus needed to solve the boundary problem.

To start the iteration process, it is necessary to set an initial pressure at the boundary. This initial value is essential as the convergence and the speed of the iterative algorithm depend on that value. In this method, the solution of the Lax-Wendroff scheme is used to initialize the pressure so the initial value is as close as possible to the solution minimizing the amount of iterations and the calculation time. Hence, the initial pressure at the boundary at each time step is set as:

$$p_D^{it} = 2p_{D-1} - p_{D-2} \quad (26)$$

Where p_D^{it} is the initial pressure for the iterative algorithm at the boundary. Equation (26) is a linear extrapolation of the pressure at the boundary using the two closest finite elements in the tube. This extrapolation can be very close to the solution, overall during the steady-state stages, avoiding the use of the iterative algorithm which decreases the calculation time.

Now that an initial pressure has been set, (21) and (24) are used to determine the values of u_D and a_D . All the information at the boundary has been found, but the coherence with respect to the outflow model as to be imposed. The non-dimensional speeds have to be calculated in order to compute (25) and find out whether the solution is consistent or not.

The knowledge of U_D and the area ratio Φ allows the pressure ratio to be computed with (25). As the back pressure is known, the pressure at the boundary obtained with the outflow model is determined when multiplying p_b by the pressure ratio previously obtained. The comparison between this pressure and the initial pressure is the criterion that determines whether p_D^{it} is a solution or not for the boundary problem. The convergence criterion can be expressed as follows:

$$f = p_D^{it} - \text{datamap}(U_1, \Phi) * p_b < \epsilon \quad (27)$$

where epsilon sets the convergence accuracy. Another important advantage of this method appears in (27) as ϵ can be defined in terms of pressure. Therefore, the convergence criterion can be easily established. However, nothing guaranties that the extrapolation used in the initial p_D^{it} satisfies the criterion of (27). That is why a iterative procedure has to be implemented until (27) is satisfied. The Newton-Raphson method has proved

to improve the performance of the inflow boundary resolution method [12] and has also been successfully used for solving the outflow boundary resolution [11]. Hence, it is proposed in this study to upgrade the value of p_D^{it} at every iteration loop.

$$p_D^{it+1} = p_D^{it} - \frac{f^{it}}{\frac{df^{it}}{dp}} \quad (28)$$

(28) describes the proposal of the NR algorithm for the outflow boundary problem. The calculation of the derivative $\frac{df^{it}}{dp}$ creates the need for generating a second data-map containing $\frac{dPR}{dU_D}$ and the computation of the remaining parts of the analytic derivative, which is inconvenient in terms of simplicity and calculation time. The numerical computation of the derivative is thus more favorable for this application. The Newton-Raphson algorithm proposed for the boundary solution is described as follows:

$$p_D^{it+1} = p_D^{it} - \frac{f(p_D^{it})}{\frac{f(p_D^{it} + \Delta p) - f(p_D^{it})}{\Delta p}} \quad (29)$$

When Δp in (29) is small, a better approximation to the analytic Newton-Raphson algorithm is obtained. This iteration procedure is only necessary under subsonic conditions. When sonic flow at Plane 2 is reached, the value of U_{Dcr} is constant independently of the pressure ratio $\frac{p_D}{p_b}$, which allows to determine U_{Dcr} and A_{Dcr} directly using equations (7) and (13) for the isentropic and momentum approaches respectively. The solution of these equations is stored in a data-map of the following form: $U_{Dcr} = \text{datamap}(\Phi)$. For sonic flow, (21) and (24) hold, therefore:

$$\frac{\lambda_L}{a_{tot}} = \frac{\gamma - 1}{2} U_D + \frac{a_L}{p_L^{\frac{\gamma-1}{2\gamma}} \sqrt{\gamma S_s^{\frac{1}{\gamma}}}} A_D \quad (30)$$

and

$$a_{tot} = \frac{\sqrt{\gamma S_s^{\frac{1}{\gamma}} p_D^{\frac{\gamma-1}{2\gamma}}}}{A_D} \quad (31)$$

Combining (30) and (31) gives:

$$p_D = \left(\frac{\lambda_L A_{Dcr}}{(A_{Dcr} + \frac{\gamma-1}{2} U_{Dcr}) \sqrt{\gamma S_s^{\frac{1}{\gamma}}}} \right)^{\frac{2\gamma}{\gamma-1}} \quad (32)$$

Using this procedure, there is no need for using an iterative algorithm for the sonic flow. At this point, all the variables under subsonic and sonic flow have been determined and the resolution method is completed.

Method implementation

To implement the subsonic method, follow the steps:

1. calculate λ_L^n and S_s^n ;
2. initialize $p_D^{it} = 2p_{D-1}^{n+1} - p_{D-2}^{n+1}$. This is the linear extrapolation using the two closest nodes inside the pipe where p_{D-1}^{n+1} and p_{D-2}^{n+1} are obtained by the Lax-Wendroff scheme,
3. use (24) to calculate a_D^{it} and (21) to compute u_D^{it}
4. calculate the total sound speed as shown in (??) and compute the non-dimensional speed U_D^{it} and A_D^{it} ;
5. compute $\frac{p_D}{p_b} = \text{datamap}(U_D^{it}, \Phi)$ using any outflow model (data-map);
6. compute (27). If $f < \epsilon$ then return $p_D^{n+1} = p_D^{it}$, $a_D^{n+1} = a_D^{it}$ and $u_D^{n+1} = u_D^{it}$. Otherwise, use (29) to update p_D^{it} and return to the step 3;

To implement the sonic method follow the steps below:

1. calculate λ_L^n and S_s^n ;
2. find U_{Dcr} with $U_{Dcr} = \text{datamap}(\Phi)$, (see (7) and (13)) and calculate A_{Dcr} using the energy conservation.
3. calculate p_D^{n+1} using (32);
4. use equation (24) to calculate a_D^{n+1} and (21) to compute u_D^{n+1} .

OUTFLOW METHOD CONVERGENCE PERFORMANCE

It is now proposed to study the convergence performance of the scheme introduced in this paper by performing a comparison with the approaches found in the literature (see Appendix I). The convergence results regarding a transient test of an intake valve are detailed. As the criterion of convergence of Benson's approach

(33) is different from the criterion of the scheme proposed in this study (27), a more general criterion is used in order to perform an objective comparison. The parameter tolerance defined by $TolX = \frac{\Delta X^{it}}{X^{it}}$ is used as a convergence criterion for both schemes. This tolerance is set to 10^{-5} for the test presented in this section.

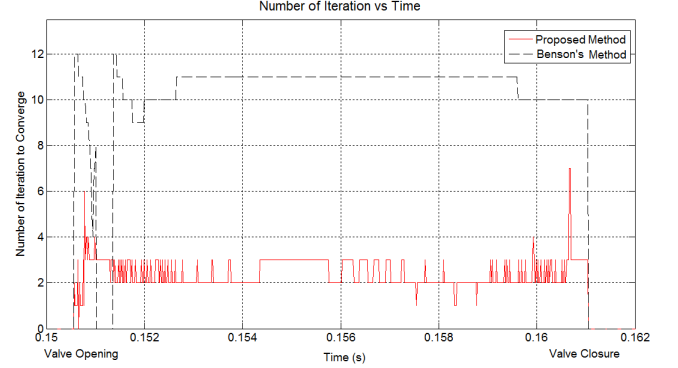


Figure 7: Comparison of number of iterations required by the literature scheme and the proposed scheme. Convergence criterion: TolX=10-5

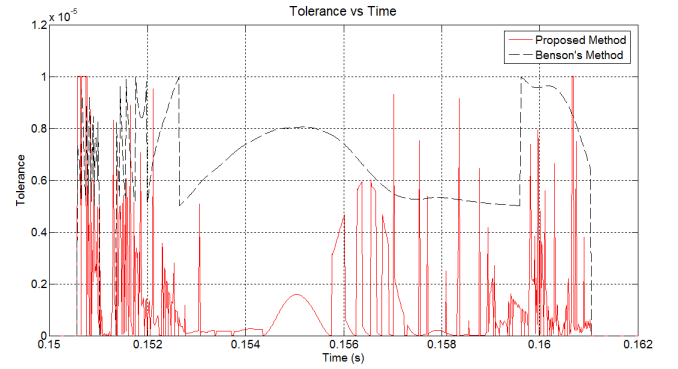


Figure 8: Accuracy obtained by the schemes

Figures 7 and 8 show the results obtained. As can be seen in Figure 7, the proposed resolution scheme provides a quicker convergence than the literature scheme: approximately 5 times faster for a tolerance of 10^{-5} . For smaller tolerances, this iteration number ratio between the schemes can increase significantly: for example for a $TolX = 10^{-6}$ the proposed scheme is 8 times faster. Figure 8 shows the final $TolX$ of the solution obtained for each scheme. It is logical that all the values are under 10^{-5} as it is the convergence criterion. However, the proposed method presents a systematically smaller criterion magnitude than the one using the literature's scheme. This behavior is due to the quadratic convergence of the Newton-Raphson method.

UNSTEADY FLOW SIMULATION VALIDATION AND RESULTS

It is important to validate the performance of the outflow boundary resolution method under unsteady flow with respect to some reference. GT-Power is used as reference for the unsteady flow validation, due to its versatility. The validation is done using the schematic presented in Figure 9.

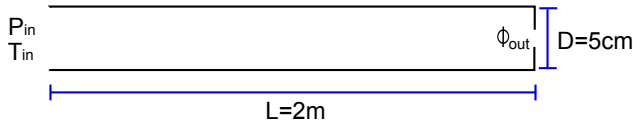


Figure 9: Scheme used for unsteady flow validation of the outflow boundary resolution method

The tube's left end, which has no restriction, is suddenly opened introducing a shock wave into the tube. p_{in} and T_{in} are set greater than the tube initial conditions inside the tube in order to generate a shock wave and test the entropy correction at the boundary, respectively. The pressure, speed and temperature are captured in the middle of the tube every time step for the validation. This experiment is reproduced in GT-Power and in a Matlab Simulink platform where the resolution scheme presented in this study has been implemented. The results are presented in Figures 10 and 11. The conditions for the test are: an initial tube pressure, speed and temperature of $10^5[\text{Pa}]$, $0[\text{m/s}]$ and $300[\text{K}]$ respectively and $p_{in} = 1.2 * 10^5[\text{Pa}]$ and $T_{in} = 500[\text{K}]$.

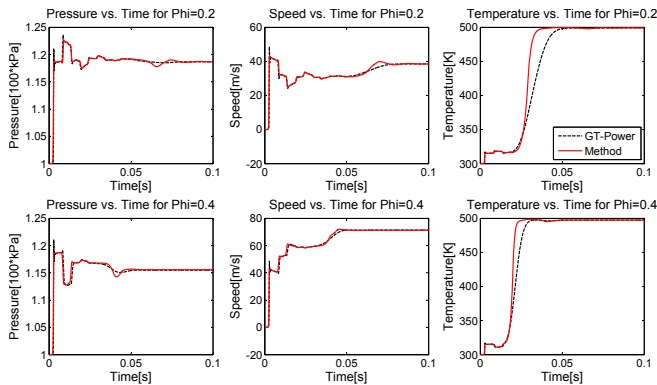


Figure 10: Scheme used for unsteady flow validation of the outflow boundary resolution method for $\Phi_{out} = 0.2$ and $\Phi_{out} = 0.4$

As it can be seen in the simulation results (Figures 10 and 11), the responses obtained with the proposed resolution method match the results obtained with GT-Power. Even when some differences between the results are appreciated due to the temperature dispersion in the GT-Power simulation, the results are satisfactory because this phenomenon is due to the

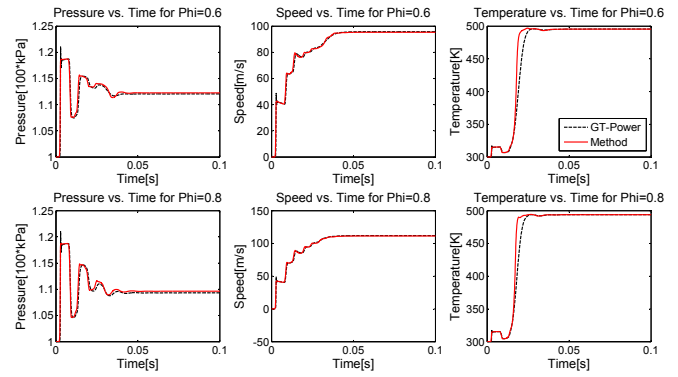


Figure 11: Scheme used for unsteady flow validation of the outflow boundary resolution for $\Phi_{out} = 0.6$ and $\Phi_{out} = 0.8$ method

GT-Power numerical scheme implemented in the tube, not in the boundary resolution method.

CONCLUSIONS

In this paper, the outflow boundary encountered at the outlet end of a tube has been studied. Two different quasi-steady outlet models have been explained in detail, and then compared with results from a 3-D CFD simulation. The momentum-based model exhibits more predictability than the traditional quasi-steady model based on the isentropic contraction assumption. This fact motivates the search of a more general boundary resolution method, able to solve the boundary problem for any quasi-steady outlet model that can be put into a data-map of the form described during this study. A modified Method of Characteristics has been used to create the interaction between the outlet models and the tube numerical scheme, always consistent with a compressible flow. The proposed resolution method allows to integrate a quasi-steady outlet model with the wave action scheme, diminishing the amount of iterations at each time step and increasing the accuracy of the response. This is due to the Newton-Raphson algorithm implemented of the iteration loop and the extrapolation used in the initialization of the boundary resolution method. The resolution scheme has been validated with GT-Power as reference, which has demonstrated the effectiveness of the proposed approach.

DEFINITIONS, ACRONYMS AND ABBREVIATIONS

- CFD:**Computational fluid dynamics
- EGR:**Exhaust gas recirculation
- HCCI:**Homogeneous charge compression ignition
- HP-EGR:**High pressure exhaust gas recirculation
- LP-EGR:**Low pressure exhaust gas recirculation
- LTC:**Low temperature combustion
- MOC:**Method of Characteristics

NR:Newton Raphon
PCCI:Premixed charge compression ignition
QSS:Quasi steady state
TVD:Time variation diminishing

[12] G. Martin, P. Brejaud, and A. Charlet P. Higelin. Pressure ratio based method for non-isentropic inflow valve boundary condition resolution. *Proceeding of the SAE conference, Paper 2010-01-1052*, 2010.

REFERENCES

- [1] K.Akihama, Y.Takatory, K.Inagaki, S.Sasaki, and A.Dean. Mechanism of the smokeless rich diesel combustion by reducing temperature. *SAE transactions-Journal of Engines, 110 Paper 2001-01-0655*, 2001.
- [2] M.Alriksson and I.Denbrant. Low temperature combustion in a heavy duty diesel engine using high levels of EGR. *Proceeding of the SAE conference, Paper 2006-01-0075*, 2006.
- [3] T.Ryan and A.Matheaus. Fuel requirements for HCCI engine operation. *SAE transactions-Journal of Fuels Lubricants, 112,1143-1152*, 2003.
- [4] A.Hribernik. The potential of the high and low-pressure exhaust gas recirculation. *Proceeding of the SAE conference, Paper 2002-04-0029*, 2002.
- [5] M.Ammann, N.Fekete, L. Guzella, and A.Glatfelder. Model-based control of the VGT and EGR in a turbocharged common-rail diesel engine: theory and passenger car implementation. *Proceeding of the SAE conference, Paper 2003-01-0357*, 2003.
- [6] J.Chauvin, G.Corde, and N.Petit. Constrained motion planning for the airpath of a diesel HCCI engine. *Proceedings of the 45th IEEE conference on decision and control, 3589-3596*, 2006.
- [7] J.Wang. Air fraction estimation for multiple combustion mode diesel engines with dual-loop EGR systems. *Control Engine Practice 16, 1479-1468*, 2008.
- [8] I.Kolmanovski, J.Sun, and M.Druzhinina. Charge control for direct injection spark ignition engines with EGR. *Proceedings of the 45th IEEE conference on decision and control, 34-38*, 2000.
- [9] R. Benson. *The Thermodynamics and Gas Dynamics of Internal-Combustion Engines*, volume Volume I. Clarenton Press-Oxford, 1982.
- [10] DE. Winterbone and RJ. Pearson. *Theory of Engine Manifold Design: Wave Action Methods for IC Engines*. Society of Automotive Engineers. Inc, 2000.
- [11] G.Martin. *0-D -1-D Modeling of the air path of ICE Engines for control purposes*. PhD thesis, Universite d'Orleans, 2009.

APPENDIX I

CLASSICAL NON-HOMETROPIC OUTFLOW BOUNDARY RESOLUTION METHOD

Subsonic flow

Benson [9] introduced a strategy to solve the homentropic outflow boundary problem based on the isentropic contraction assumption. The method can be modified to solve the non-homentropic cases by the introduction of the "starred Riemann variables". In this section, only the basic procedure is presented. Benson's resolution method for sub-sonic flow is based on the solution of:

$$f(A) = \left(A^{\frac{4}{\gamma-1}} - \Phi^2 \right) (\lambda - A)^2 - \frac{\gamma-1}{2} (A^2 - 1) \Phi^2 = 0 \quad (33)$$

at every time step. The remaining quantities at the boundary are found using the following equations

$$U = \frac{2}{\gamma-1} (\lambda - A) \quad (34)$$

And

$$A = \left(\frac{p}{p_{ref}} \right)^{\frac{\gamma-1}{2\gamma}} \quad (35)$$

Different solution methods for 33 have been proposed. Benson proposed the following method:

1. the algorithm is initialized at $A_n = \frac{\lambda+1}{2}$ as the solution is in the range $[1, \lambda]$;
2. the initial step is defined as $\Delta A_n = \frac{\lambda-1}{4}$
3. (33) is evaluated using A_n :
 if $f(A) < 0$ then set $A_{n+1} = A_n - \Delta A_n$ else set $A_{n+1} = A_n + \Delta A_n$;

4. if $f(A) < \epsilon$ then return A ,
 else set $\Delta A_{n+1} = \frac{\Delta A_n}{2}$ and $A_n = A_{n+1}$. Go back to step 3.

Martin proposed to use a Newton-Raphson algorithm to solve equation 33 instead of the iterative method of Benson [11]. His method introduces a polytropic coefficient to model the non-homentropic cases that is obtained by data-maps. However, the method does not improve significantly the calculation time and it does not take into account the change of entropy level at the boundary. The procedure is described as follows:

1. the algorithm is initialized at $A_n = \frac{\lambda+1}{2}$ as the solution is in the range $[1, \lambda]$;
2. using the energy equation $1 = A_n^2 + \frac{\gamma-1}{2} U_n^2$, the value of U_n is determined;
3. the polytropic coefficient is found using a data-map of κ versus λ/a_0 , where $a_0 = \frac{\lambda}{A_n + \frac{\gamma-1}{2} U_n}$;
4. now that κ , A_n and λ are known, (33) is evaluated. If $f(A) < \epsilon$ the solution has converged. Else the Newton-Raphson algorithm is introduced in order to update the value of A_n . It is run until the solution is converged.

Sonic flow

When the flow in the throat is choked there is a sonic flow. As seen in the previous section, the model equations change as well as the resolution method does when a sonic flow occurs. Benson proposed a solution method based on the solution of the following equation (the same approach is done in [11]):

$$f\left(\frac{A}{A_t}\right)_{cr} = \Phi^2 - \left[\frac{\gamma+1}{\gamma-1} - \left(\frac{2}{\gamma-1}\right) \left(\frac{A}{A_t}\right)_{cr}^2 \right] \left(\frac{A}{A_t}\right)_{cr}^{\frac{4}{\gamma-1}} \quad (36)$$

This equation cannot be solved analytically, therefore another numerical method has to be introduced.